JACS
JOURNAL OF THE AMERICAN CHEMICAL SOCIETY
Article
pubs.acs.org/JACS

A Photocatalyst–Enzyme Coupled Artificial Photosynthesis System for Solar Energy in Production of Formic Acid from CO_2

Rajesh K. Yadav,[†] Jin-Ook Baeg,*[,†] Gyu Hwan Oh,[†] No-Joong Park,[†] Ki-jeong Kong,[†] Jinheung Kim,[‡] Dong Won Hwang,[†] and Soumya K. Biswas[†]

[†]Advanced Chemical Technology Division, Korea Research Institute of Chemical Technology, 100 Jang-dong, Yuseong, Daejon, 305-600, Republic of Korea

[‡]Department of Chemistry and Nano Science, Ewha Womans University, 11-1 Daehyun-dong, Seodaemun-gu, Seoul, 120-750, Republic of Korea

Supporting Information

ABSTRACT: The photocatalyst–enzyme coupled system for artificial photosynthesis process is one of the most promising methods of solar energy conversion for the synthesis of organic chemicals or fuel. Here we report the synthesis of a novel graphene-based visible light active photocatalyst which covalently bonded the chromophore, such as multianthraquinone substituted porphyrin with the chemically converted graphene as a photocatalyst of the artificial photosynthesis system for an efficient photosynthetic production of formic acid from CO_2. The results not only show a benchmark example of the graphene-based material used as a photocatalyst in general artificial photosynthesis but also the benchmark example of the selective production system of solar chemicals/solar fuel directly from CO_2.

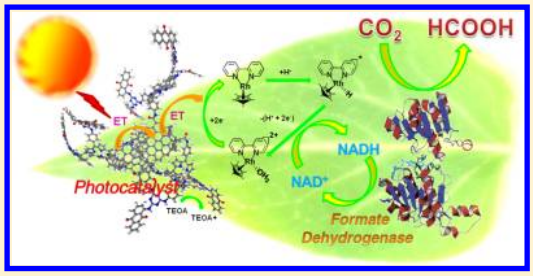

1. INTRODUCTION

The direct conversion of solar energy into chemical energy for the production of renewable and nonpolluting fuels remains a great and fascinating challenge for this century. One of the most promising methods of solar energy conversion for the synthesis of organic chemicals or fuel is artificial photosynthesis.[1−3] Many approaches to artificial photosynthesis have been explored, and some of these employ photocatalysts, such as semiconductors, transition-metal complexes, and so on. Although photocatalytic artificial photosynthesis has proved to be feasible, many problems still remain, such as low conversion efficiency, low selectivity of products, and stability problems of the photocatalyst when conventional setups are used.[4]

In an earlier work, we reported $W_2Fe_4Ta_2O_{17}$ to be a photocatalyst for a photocatalyst–enzyme coupled system.[5] The photocatalyst–enzyme coupled system is one of the most ideal artificial photosynthesis systems which utilizes solar energy for the synthesis of various chemicals and fuel. For practical use of the photocatalyst–enzyme coupled artificial photosynthesis process, one of the most challenging tasks is the search for a highly efficient visible light active material which acts as a photocatalyst in the reduced nicotinamide adenine dinucleotide (NADH) regeneration system and triggers enzymatic production of solar chemicals/solar fuel from CO_2.[5] Since energetically 46% of the total solar light available on earth is in the visible range and only 4% is in the UV range,[6] it is imperative that the photocatalysis must be visible light functional for real and meaningful solar energy conversion.

Graphene has proved to be a mounting superstar in the fields of material science, condensed-matter physics, and chemistry[7,8] having remarkable electronic, thermal, optical, and mechanical properties.[9,10]

Recently, there are some reported examples of graphene and photocatalyst composite. They are simple composites of metal oxide semiconductor photocatalyst, such as TiO_2 and graphene.[11,12] But the graphene and metal oxide semiconductor composite could not be suitable as a photocatalyst for the photocatalyst–biocatalyst coupled system because of intrinsic low-energy level of the conduction band edges.

The small energy difference between the conduction band edges of metal oxide and the reduction potential of rhodium complex makes it difficult to transfer the photoexcited electrons in the metal oxide into the reduction center and finally results in very low efficiency of the NADH regeneration.

Here we report the synthesis of a novel graphene-based visible light active photocatalyst which covalently bonded the chromophore, such as multianthraquinone substituted porphyrin (MAQSP) with the chemically converted graphene (CCG)[13] as a photocatalyst of the photocatalyst–enzyme coupled system for an efficient artificial photosynthetic production of formic acid from CO_2. The results not only show a benchmark example of the graphene-based material used as a photocatalyst in general artificial photosynthesis but also the benchmark example of the selective production system of solar chemicals/solar fuel directly from CO_2.

Received: January 31, 2012
Published: July 6, 2012

   dx.doi.org/10.1021/ja3009902 | J. Am. Chem. Soc. 2012, 134, 11455–11461

2. RESULTS AND DISCUSSION

2.1. A Photocatalyst−Biocatalyst Coupled Artificial Photosynthesis System. A diagrammatic representation of the photocatalyst−biocatalyst coupled system based on the synchronized working mechanism of photocatalysis and biocatalysis involved in the formation of formic acid from CO_2 is shown in Scheme 1.

Scheme 1. Graphene-Based Photocatalyst Catalyzed Artificial Photosynthesis of Formic Acid From CO_2 under Visible Light

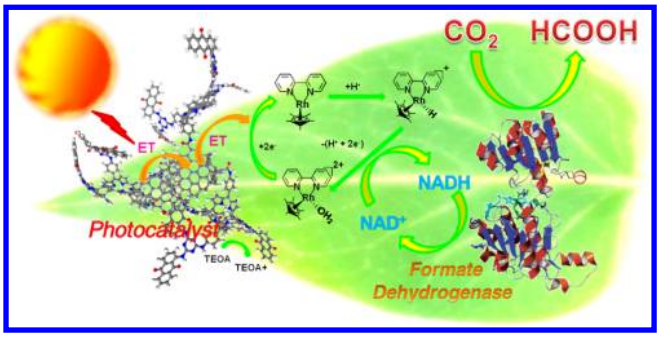

The graphene-based photocatalyst is a material which covalently bonded the chromophore (as an electron donor), such as anthraquinone substituted porphyrin with the chemically converted graphene (as an electron acceptor). The absorption of photon occurs as a transition between localized orbitals around chromophore (MAQSP). The created electrons reach to the rhodium complex via graphene. An organometallic rhodium complex easily receives the electron and is reduced.[14] It further abstracts a proton from aqueous solution and transfers electrons and a hydride to NAD^+, which gets converted to NADH thus forming the photocatalysis cycle.[5] In this way, the rhodium complex shuttles as an electron mediator between the graphene photocatalyst and NAD^+, proving as an efficient factor for regeneration of the NADH cofactor. Finally, NADH is consumed by the CO_2 substrate for its enzymatic (formate dehydrogenase) conversion to formic acid. The NAD^+ released from the enzyme can undergo photocatalysis cycle in the same way, leading to the photoregeneration of NADH. These two catalysis cycles thus couple integrally to work together, ultimately yielding formic acid from CO_2.

The chemically converted graphene coupled multianthraquinone substituted porphyrin (CCGCMAQSP) used as a photocatalyst in the photobioreactor was synthesized via multistep synthesis involving the substitution of 1-aminoanthraquinone moieties (AAQ) linked by 1,3,5-trichlorotriazine (TCT) units to a 5,10,15,20-tetrakis(4-aminophenyl)porphyrin (TkisAPP) core to enhance the efficiency of light energy harvesting.

2.2. Characterization of Graphene-Based Photocatalyst. The XRD (Model: Rigaku D/Max-2200 V X-ray diffractometer and Cu Kα radiation) pattern of CCG exhibits a weak and broad characteristic peak of CCG which appeared at the 2θ value of 22.5°. The peak at 22.5° corresponds to the interlayer spacing (d-spacing) in CCG of about 0.39484 nm which is very close to that of naturally available graphite, 0.335 nm.[13] The slightly higher value of this interlayer distance in CCG compared to that in graphite indicates the presence of a small amount of −COOH groups[15] remaining in CCG which participate in the formation of a new −CONH− bond with MAQSP.

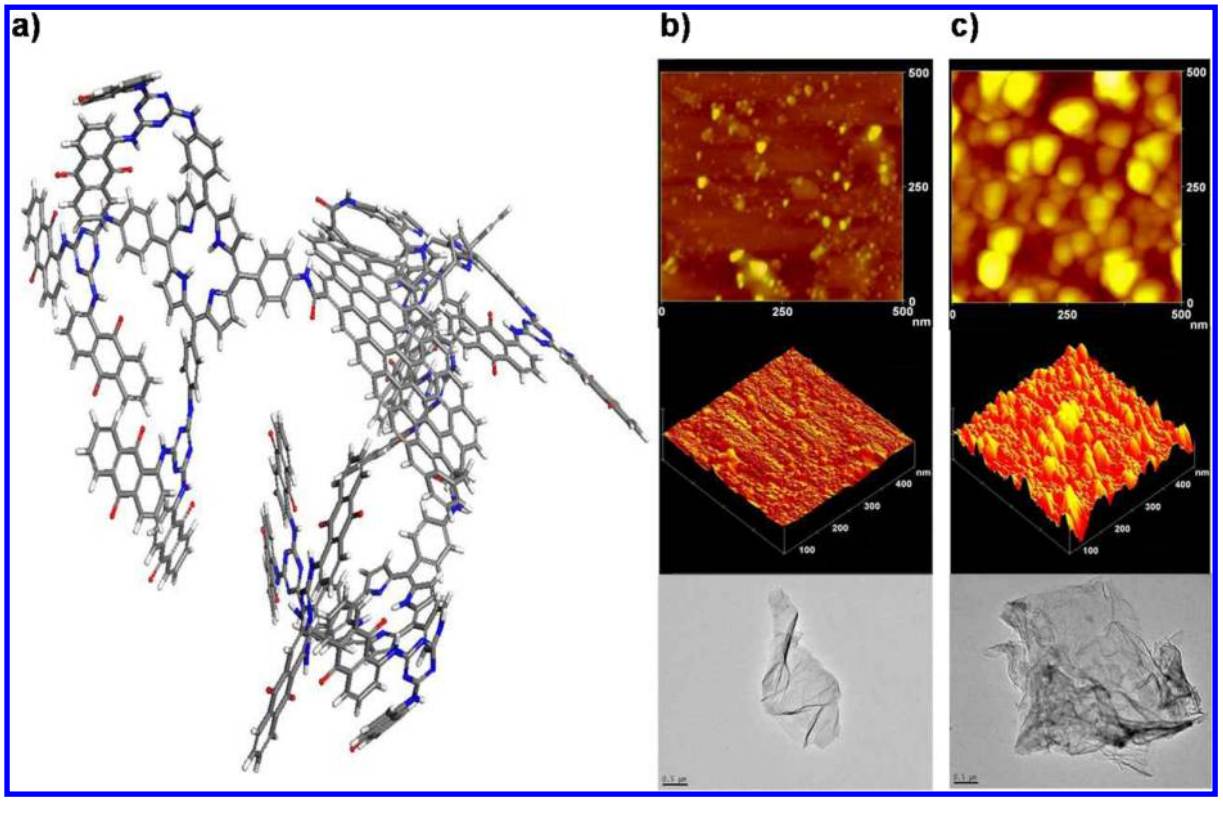

Figure 1. (a) 3D structure of the graphene-based photocatalyst (CCGCMAQSP). AFM and TEM images of (b) CCG and (c) CCGCMAQSP.

dx.doi.org/10.1021/ja3009902 | J. Am. Chem. Soc. 2012, 134, 11455−11461

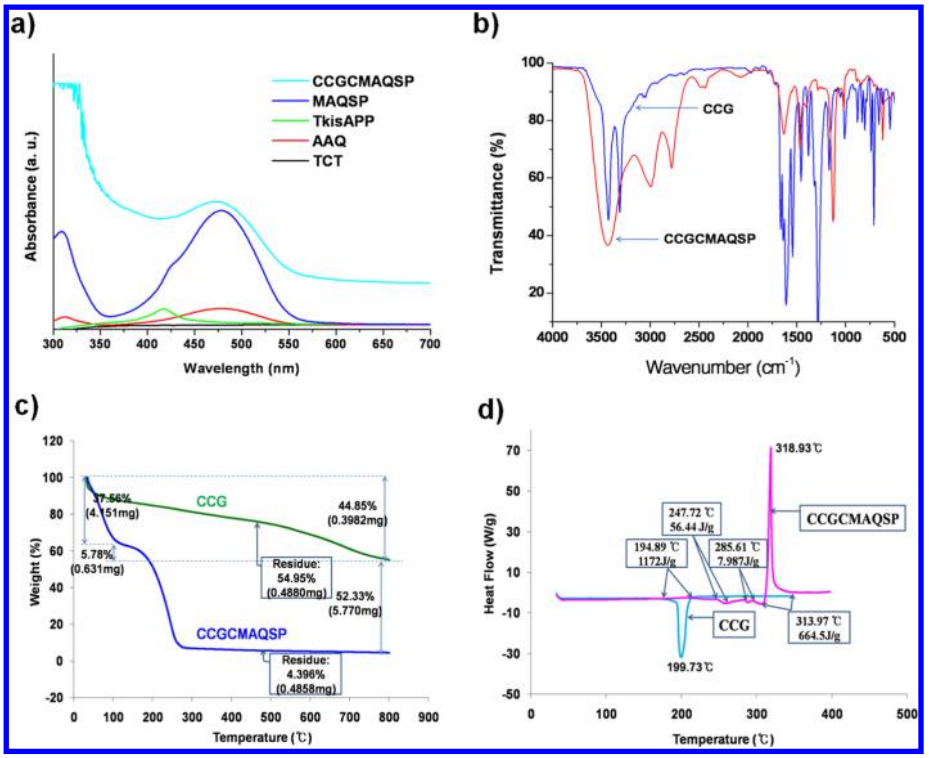

Figure 2. (a) UV absorption spectroscopy of CCGCMAQSP, MAQSP, TkisAPP, AAQ, and TCT. (b) FTIR spectra of CCG and CCGCMAQSP. (c) TGA of the CCG and CCGCMAQSP. (d) DSC of the CCG and CCGCMAQSP.

Formation of the proposed photocatalyst, CCGCMAQSP, through generation of the −CONH− bond by the coupling reaction between CCG and MAQSP is suggested by the appearance of a weak and broad peak at the 2θ value of 23.5° in the XRD of CCGCMAQSP (see Supporting Information).

Figure 1 shows 3D structure of the graphene-based photocatalyst (CCGCMAQSP) and atomic force microscopy (AFM) and TEM images of the CCG and CCGCMAQSP.

The graphene (CCG) and the photocatalyst (CCGMAQSP) were imaged using AFM as shown in Figure 1b,c and Figure S1, Supporting Information. The samples for AFM investigations were prepared by ultrasonic treatment of CCG and CCGMAQSP (in DMF) dispersions of 0.0003 g/L. The samples were prepared through drop-casting on a cleaned glass surface. The roughness of CCG and CCGMAQSP are 1.156 and 1.836 nm (Figure 1b and 1c). The thickness of CCG and CCGMAQSP are 1.194 nm and 1.997 nm (Figure S1. a and b, see Supporting Information). It depicts that the edge of CCG has been roughened by the coverage of soft material indicating the presence of covalently attached MAQSP. The morphology of synthesized CCG and CCGCMAQSP was also characterized by AFM and TEM (Figure 1b,c). The TEM (Figure 1b) result indicated that the CCG existed in the single layer. Surface morphology of CCG (AFM and TEM, Figure 1b) also has been changed after the covalently attached MAQSP (AFM and TEM, Figure 1c). The topographical height of CCGMAQSP 1.997 nm is also attributed to covalently linked MAQSP to CCG.[16]

The UV absorption studies of TCT, AAQ, TkisAPP, MAQSP, and CCGCMAQSP have been conducted in DMF. CCGCMAQSP (Figure 2a) showed a strong Soret band absorption at 475 nm, which is consistent with that of MAQSP. This type of observation has been already reported.[17] TCT, AAQ, TkisAPP, and MAQSP exhibit low absorption near 300 nm, while CCGCMAQSP exhibits higher absorption at the same range.

This demonstrates that in the ground-state attachment of the MAQSP core has relaxed the electronic properties of CCG thereby proving the high efficiency of CCGCMAQSP as a photocatalytic energy for NADH regeneration, which is indispensable in the enzymatic production of solar chemicals/fuels from CO_2.

The FTIR (Bruker, ALPHA-T FT-IR spectrometer) studies gave a clear evidence for the coupling of MAQSP with CCG and the reduction of CCG. The inset shows prolonged plots of the CCG (Figure 2b) spectra from 1000 to 1750 cm^{-1}. The spectra show important bands around 1060 cm^{-1} ($^{\nu}$C−O), 1220 cm^{-1} ($^{\nu}$phenolic), 1370 cm^{-1}($^{\nu}$O−H bending in tertiary alcohol), 1620 cm^{-1} ($^{\nu}$HOH bending in water), and 1720 cm^{-1} ($^{\nu}$C═O).

After reduction these peaks disappear, and a new peak appears at 1705 cm^{-1}, which is obvious in CCG. In the spectrum of CCGCMAQSP, the peak at 1705 cm^{-1} almost disappears, and a new broad band emerges at 1617 cm^{-1}, which corresponds to the C═O characteristic stretching band of the amide group (−NHCO−). The C−N stretching band of the amide group which appears at 1235 cm^{-1} clearly indicates the presence of amide linkage (−NHCO−) in the structure, thereby showing the coupling of MAQSP with CCG.

The thermal behavior of CCG and CCGCMAQSP was investigated by thermogravimetric analysis (TGA, model: Q 500) (Figure 2c) in the temperature range from 25 to 900 °C and differential scanning calorimetry (DSC, model: 2910) (Figure 2d) at a heating rate of 5 °C min^{-1} under Ar flow in the temperature range from 25 to 400 °C. CCG exhibits slow weight loss with an increase of temperature up to 800 °C. The TGA curve for CCGCMAQSP shows a two-step weight loss. A steady weight loss up to 37.56% in the temperature range from

dx.doi.org/10.1021/ja3009902 | J. Am. Chem. Soc. 2012, 134, 11455−11461

25 °C to ~100 °C corresponds to the typical pattern of sidewall functionalization. This is followed by the second major weight loss in the temperature range from 180 to 380 °C with an exothermic peak appearing at around 340 °C in the DSC curve (Figure 2d), indicating the breaking of the amide bonds within the MAQSP system.[18]

For confirmation of the coupling of MAQSP with CCG and the restoration of CCG to CCGCMAQSP in the existence of MAQSP were carried out by Raman (model: Bruker/SENTERRA) and by XPS (model: KARTOS AXIS NOVA), respectively (see Supporting Information). In uncorroded single-layer graphene, the disorder band of 1350 cm^{-1} was hardly noticeable, but the 1350 cm^{-1} mode consequently developed after the oxidation began. There is a practical correlation between the intensity (I) ratio of the 1350 cm^{-1} mode to that of the 1625 cm^{-1} mode (I_{1350}/I_{1625}) as reported elsewhere.[19] From the Raman spectra, it is obvious that the insignificant (I_{1350}/I_{1625}) ratio reveals the singularity of the CCG layer. Moreover, coupling of CCG with MAQSP leads to a shift in the band (see Supporting Information). The incorporation of MAQSP into the CCG material leads to a prominent Raman shift in the 2000−500 cm^{-1} region. We observed considerable shifts at the 1350 and 1625 cm^{-1} bands of the spectra of CCGCMAQSP at 500 and 1125 cm^{-1}, respectively.

Energy-dispersive X-ray spectroscopy (EDS, model: Bruker/Quantax 200) analysis showed that CCG is composed of carbon (73.12 atom %), oxygen (26.28 atom %), and MAQSP samples with carbon (68.29 atom %), oxygen (11.78 atom %), and nitrogen (19.93 atom %), respectively. Furthermore, the impurity of unwanted materials is undetectable in the sample as shown in the Supporting Information data. It is apparent that the CCG becomes smoother after the attachment of MAQSP, and the ratio of the CCGCMAQSP contents (O/C) is somewhat lower than that of CCG as a result of the presence of nitrogen.[20]

The BET surface area of CCG (254 $m^2\ g^{-1}$) is very close to the reported value.[21] The BET measurement of CCGMAQSP (189.01 $m^2\ g^{-1}$) gives a little lower value than CCG, which is due to the MAQSP on the CCG.

2.3. Photoelectrochemical Measurement. Transient photocurrent were measured on a photoelectrochemical test device fabricated by drop-casting the covalently attached CCGCMAQSP hybrid material dispersed in ethanol (0.09 g/mL) onto fluorine-doped tin oxide (FTO) coated glass. The Figure 3 shows the photocurrent response versus time of MAQSP and CCGCMAQSP photocatalyst. It is found that the photocurrent of the CCGCMAQSP photocatalyst is much higher than MAQSP. The photocurrent response of the CCGCMAQSP hybrid material is reasonably reversible and stable, from which we can see that the current can reproducibly increase severely under each irradiation and quickly recover in the dark. The stable photocurrent property of our photocatalyst (CCGCMAQSP) is also in agreement with many observations for graphene hybrid materials and composites, which showed a stable photocurrent.[22,23] Therefore the observed photocurrent represents charge transportation through a photocatalyst (CCGCMAQSP) to the collecting electrode (FTO glass) surface.[24]

2.4. Photocatalytic NADH Regeneration and Photosynthetic Production of Formic Acid from CO_2. A series of photocatalysis experiments was performed to study the photocatalytic activities of $W_2Fe_4Ta_2O_{17}$,[5] MAQSP, and CCGCMAQSP for the visible light-driven photoregeneration of NADH. The concentration of photoregenerated NADH was measured by spectrophotometer.[5] As shown in Figure 4, CCGCMAQSP is significantly effective for NADH photoregeneration constantly accumulated up to 45.54% with a time linearity. However, $W_2Fe_4Ta_2O_{17}$ photocatalyst and MAQSP

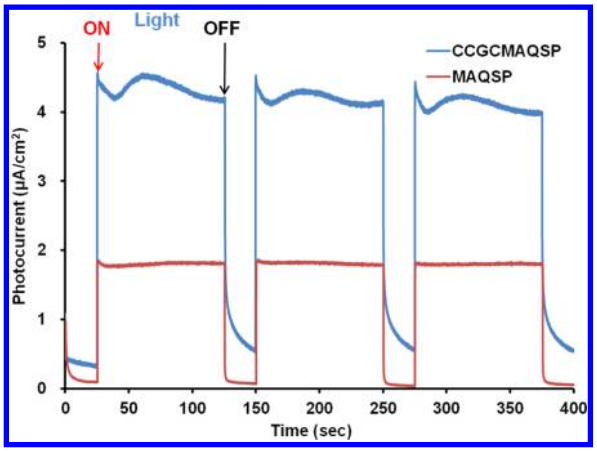

Figure 3. Photocurrent response of FTO/CCGCMAQSP and FTO/MAQSP electrode under illumination of simulated sun light [1sun] (three electrodes; platinum counter electrode, Ag/AgCl reference electrode, glassy carbon working electrode, 0.1 M NaCl aqueous solution containing 0.4 M TEOA as a redox couple/electrolyte and scan rate of 100 mV/s).

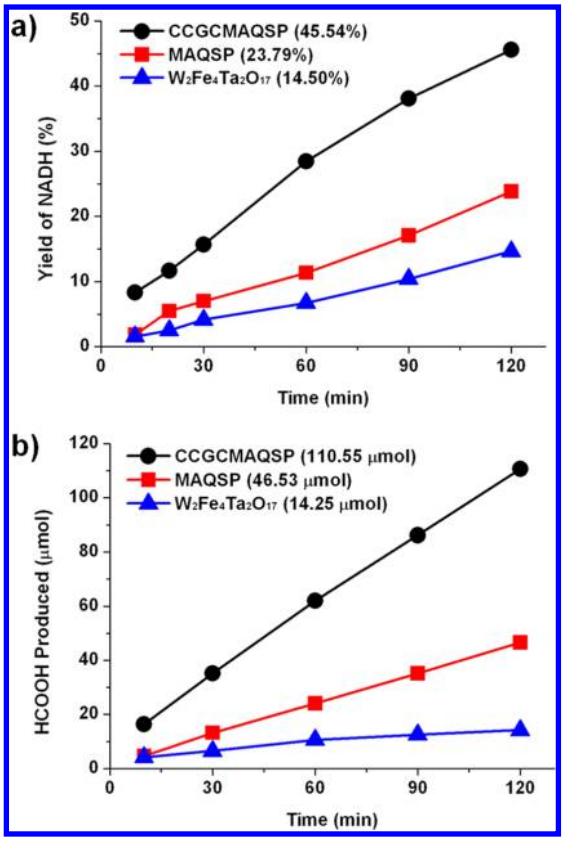

Figure 4. Photocatalytic activities of CCGCMAQSP, MAQSP, and $W_2Fe_4Ta_2O_{17}$ in NADH photoregeneration and visible-light driven artificial photosynthesis of formic acid from CO_2. (a) NADH photoregeneration and (b) visible-light driven artificial photosynthesis of formic acid from CO_2.

dx.doi.org/10.1021/ja3009902 | J. Am. Chem. Soc. 2012, 134, 11455−11461

give only 14.50% and 23.79% yield of NADH regeneration, respectively (Figure 4a).

Additional experiments were performed to study the photocatalytic performance of $W_2Fe_4Ta_2O_{17}$, MAQSP, and CCGCMAQSP for the visible light-driven artificial photosynthesis of formic acid from CO_2. The amount of formic acid was detected by GC (7890A, Agilent Technologies). As shown in Figure 4b, the formic acid yield increases linearly with the reaction time when CCGCMAQSP is used as a photocatalyst. The efficiency of CCGCMAQSP for the production of formic acid for 2 h was 110.55 μmol, while $W_2Fe_4Ta_2O_{17}$ and MAQSP were 14.25 and 46.53 μmol, respectively. These investigations clearly reveal the superiority of the graphene-based photocatalyst (CCGCMAQSP) over the other photocatalysts.

To elucidate the origin of the photocatalytic activity and the activity enhancement of the graphene-based photocatalyst (CCGCMAQSP), we have performed a series of first-principles calculations using plane-wave-based density functional theory (DFT) code, VASP.[25] To overcome the computational limit imposed by the large size of molecular system, we divided the CCGCMAQSP into two parts, CCG composed of 30 hexagon rings and MAQSP, which were saturated by carboxyl and amine groups, respectively, and then performed electronic structure calculations separately (Figure 5).

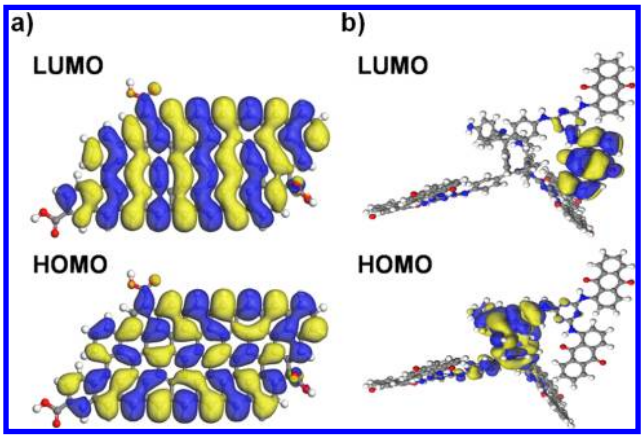

Figure 5. Visualization of the molecular orbitals (LUMO and HOMO) of the (a) CCG and (b) MAQSP as obtained at the DFT-GGA level of approximation.

It is well-known that the Kohn–Sham eigenvalues obtained in DFT should not be directly interpreted as electron removal/addition energies because the method does not satisfy Koopman's theorem.[26] However, DFT results can give clues regarding the peak shift of optical absorption and the direction of electron transport.

The incident light is absorbed at MAQSP, where photoexcitation occurs, and the created electrons move into the CCG via a stable amide bond. The electron-transfer efficiency could be estimated by the energy level alignment between the conduction band edges of CCG and the lowest unoccupied molecular orbital (LUMO) of MAQSP. From our DFT calculation results, we have confirmed that the energy level of each segment is aligned for electrons to transfer from MAQSP finally to hydrogen reduction site via CCG. The Fermi level of graphene, which is calculated to be 4.14 eV lower than vacuum level, lies at the center of bandgap of MAQSP. The calculated bandgap of MAQSP is ~0.6. By the usage of triethanolamine (TEOA)as a hole scavenger, the electron transfer from CCG to the photoexcited MAQSP is forbidden. Thus, the photoexcited electrons created in MAQSP can be easily transferred into CCG, not reversely. The huge surface area and the extremely high carrier mobility of graphene[27] raise the probability for electrons to be transferred into rhodium complex, eventually accelerating the chemical reactions of NADH generation. Furthermore, the graphene also acts as an electron reservoir to transport multiple electrons. In most molecular systems, the energy cost of electron addition is very high because of large Coulomb repulsion between localized electrons. In graphene, the multielectron addition or removal can be possible because of the delocalized nature of wave functions over the whole graphene surface (extending several μm).

3. CONCLUSION

In summary, we presented here a new graphene-based photocatalyst (CCGCMAQSP) for artificial photosynthesis. The photocatalyst (CCGCMAQSP) has been fully characterized through spectroscopy, thermal analysis, and microscopy. Moreover, photoelectrochemical studies together with DFT calculation have allowed the evaluation of photoelectrochemical property and the origin of the photocatalytic activity of the photocatalyst. The CCGCMAQSP is a highly active visible light photocatalyst of the photocatalyst–enzyme coupled system for an efficient artificial photosynthetic production of formic acid from CO_2. This opens possibilities of applications for graphene-based materials, especially in the field of artificial photosynthesis. One of the most challenging tasks for practical use of the photocatalyst–biocatalyst coupled system for artificial photosynthesis process is the search for a highly efficient visible light active material which acts as a photocatalyst in the NADH regeneration system and triggers enzymatic production of solar chemicals/solar fuel from CO_2. Thus, the present work demonstrates successfully a new and promising the graphene-photocatalyst-based artificial photosynthetic system for the ultimate goal of solar energy utilization in tailor-made synthesis of fine chemicals and solar fuel from CO_2.

4. EXPERIMENTAL SECTION

4.1. Materials. All chemicals were purchased from Aldrich. Enzyme (formate dehydrogenase) and β-nicotinamide adenine dinucleotide (β-NAD) were purchased from Sigma. Graphite powder (99.9995%, 325 mesh) was purchased from Alfa Aesar.

4.2. Synthesis of Graphene Oxide. The graphene oxide was prepared according to reported method:[28] Into 0.115 L of sulfuric acid, 5.0 g of powdered graphite (325 mesh) and 2.5 g of sodium nitrate were added. The ingredients were mixed in a 10 L battery jar that had been cooled to 0 °C in an ice bath as a safety measure. While maintaining vigorous agitation, 15.0 g of potassium permanganate was added to the suspension. The rate of addition was controlled carefully to prevent the temperature of the suspension from exceeding 20 °C. The ice bath was then removed, and the temperature of the suspension brought to 35 °C for 30 min. As the reaction progressed, the mixture gradually thickened and effervescence ceased. At the end of 20 min, the mixture became brownish gray paste with evolution of only a small amount of gas. After 30 min, 2.3 L of water was slowly stirred into the paste, causing violent effervescence and an increase in temperature to 98 °C. The diluted suspension was maintained at this temperature for 15 min. The suspension was then further diluted to approximately 7 L of warm water and treated with hydrogen peroxide to reduce the residual permanganate and manganese dioxide to colorless soluble manganese sulfate. Upon treatment with the peroxide, the suspension turned bright yellow. The suspension was filtered resulting in a yellow-brown, i.e., cake type. The filtering was conducted while the suspension was still warm to avoid precipitation of the slightly soluble

dx.doi.org/10.1021/ja3009902 | J. Am. Chem. Soc. 2012, 134, 11455–11461

salt of mellitic acid formed as a side reaction. After washing the yellowish-brown filter cake three times with a total of 7 L of warm water, the graphitic oxide residue was dispersed in 16 L of water to approximately 0.285 g solid. The remaining salt impurities were removed by treating with resinous anion and cation exchangers. The dry form of graphitic oxide was obtained by centrifugation followed by dehydration at 40 °C over phosphorus pentoxide.[15]

4.3. Preparation of Chemically Converted Graphene from Graphene Oxide. For the reduction procedure, dry graphene oxide was dispersed in deionized water to give a colloidal solution. The pH of this solution was adjusted to 9−10. Sodium borohydride was directly added into the solution of graphene oxide dispersion under magnetic stirring, and the mixture was kept at 80 °C for 1 h with constant stirring. The reduced product was filtrated and washed with large amounts of water several times to remove most residual ions. This moderately reduced graphene oxide was kept in vacuum desiccators with phosphorus pentoxide for two days, redispersed in concentrated sulfuric acid, and heated to 120 °C with stirring for 12 h. After cooling down, the dispersion was diluted with deionized water. The final product was separated by filtration.[15]

4.4. Preparation of 5,10,15-[(4-{(3,5-Tris-(dichlorotriazine)}-aminophenyl)-20-aminophenyl porphyrin] Synthesis of 5,10,15-[(4-{(3,5-Tris-(diamino-anthraquinone)triazine}-inophenyl)-20-aminophenyl porphyrin]. A solution of 5,10,15-[(4-{(3, 5-Tris-(dichlorotriazine)}aminophenyl)-20-aminophenyl porphyrin] in THF, amino-anthraquinone (6 mmol), and triethylamine (6.6 mmol) was added and stirried at 80 °C for 10 h. The completion of the reaction was monitored by thin-layer chromatography (TLC). The solvent was removed, and the residue was purified by column chromatography on silica gel using CH_2Cl_2/ethyl acetate (50:1 v/v) as eluent. The title compound was isolated 53% yield. 1H NMR (CGCl3, δ in ppm): 9.31 (s, $9H_{\text{aromatic secondary amine}}$), 9.13 (d, $6H_g$), 8.70 (s, $8H_{\text{pyrrol}}$), 8.67(m, $18H_{f+c+b}$), 8.51 (m, $18H_{a+d+e}$), 8.46 (d, $8H_{i+k}$, J = 6.6 Hz), 7.72 (d, $8H_{h+j}$), 4.20 (s, $2H_{\text{amine}}$), −2.78 (s, $2H_{\text{pyrrol−NH}}$); LC/MS, ESI (m/z): 2237.78 (M^+).[29,30]

4.5. Preparation of CCGCMAQSP. CCG (50 mg) and MAQSP[29] (150 mg) were stirred in DMF (50 mL) in the presence of a catalytic amount of triethylamine (1 mL) at 130 °C for 3 days under argon. The round bottle flask was removed from oil bath and cooled at room temperature, and ether (1.5 L) was added to precipitate out the product. The product was filtered on a membrane filter paper. The excess unwanted MAQSP and other impurities were removed through multiple washing with water, followed by sonication, filtration, and resuspension of the solid in tetrahydrofuran (500 mL). The crude product was again washed with $CHCl_3/CH_2Cl_2$ many times, via the same above procedure. UV spectroscopy and TLC were used to check the filtrate to make sure no MAQSP existed in the final washing. The CCGCMAQSP was then washed with a small amount of H_2O to remove acid−amine impurities, and eventually dried under vacuum to yield the hybrid CCGCMAQSP.[28,30] The photocatalyst (CCGCMAQSP) was analyzed by AFM, FTIR, TGA, DSC, XRD, Raman spectra, XPS, and energy-dispersive X-ray spectroscopy (see Supporting Information).

4.6. Photoelectrochemical Measurements. Photoelectrochemical measurements were carried out in a three-armed cell consisting of reference (Ag/AgCl, BASI, MF-2063 RE-5), working (CCGCMAQSP photoanode), and platinum wire (part no.: CHI115) counter electrodes using a electrochemical analyzer CHI Instruments 1100A. A 0.1 M NaCl solution containing 0.4 M TEOA was used as a redox couple/electrolyte. Newport solar simulator (69911) was used as a light source. Light intensity was measured by VSLI standard incorporated Oriel P/N 91150 V.

4.7. Photochemical Regeneration of NADH. The photochemical regeneration of NADH was performed within a quartz reactor under an inert atmosphere at room temperature, and a 450 W xenon lamp (Newport 66921) with a 420 nm cutoff filter was used as a light source. The photocatalytic regeneration of NADH was carried out as follows. The reaction was performed in a quartz reactor. The reaction was composed with β-NAD (1.24 μmol), rhodium complex (0.62 μmol), TEOA (1.24 mmol), and photocatalyst (0.5 mg) in 3.1 mL of sodium phosphate buffer (100 mM, pH 7.0). The regeneration of NADH was monitored by a spectrophotometer (UV-1800, Shimadzu).

4.8. Artificial Photosynthesis of Formic Acid from CO_2. The artificial photosynthesis of formic acid from CO_2 was also performed within a quartz reactor under an inert atmosphere at room temperature, and a 450 W xenon lamp with a 420 nm cutoff-filter was used as a light source. The reaction was composed of photocatalyst (0.5 mg), β-NAD (1.24 μmol), rhodium complex (0.62 μmol), and formate dehydrogenase (3 units) in 3.1 mL of sodium phosphate buffer (100 mM, pH 7.0) with TEOA (1.24 mmol) in the presence of CO_2 (flow rate: 0.5 mL/min). After bubbling of CO_2 for 1 h without light (light off), the reactor was exposed to visible light (light on). The amount of formic acid was detected by GC (7890A, Agilent Technologies).

■ ASSOCIATED CONTENT

Ⓢ Supporting Information

Synthesis of CCGCMAQSP scheme, XRD, RAMAN, and XPS data available. This material is available free of charge via the Internet at http://pubs.acs.org.

■ AUTHOR INFORMATION

Corresponding Author

jobaeg@krict.re.kr

Notes

The authors declare no competing financial interest.

■ ACKNOWLEDGMENTS

This work was supported by the KRICT 2020 project program.

■ REFERENCES

(1) Yfrach, G. S.; Liddell, P. A.; Hung, S. C.; Moore, A. L.; Gust, D.; Moore, T. A. *Nature* **1997**, *385*, 239−241.

(2) Yfrach, G. S.; Rigaud, J. L.; Durantini, E. N.; Moore, A. L.; Gust, D.; Moore, T. A. *Nature* **1998**, *392*, 479−482.

(3) Listorti, A.; Durrant, J.; Barber, J. *Nat. Mater.* **2009**, *8*, 929−930.

(4) (a) Roy, S. C.; Varghese, O. K.; Paulose, M.; Grimes, C. A. *ACS Nano* **2010**, *4*, 1259−1278. (b) Gust, D.; Moore, T. A.; Moore, A. L. *Faraday Discuss.* **2012**, *155*, 9−26.

(5) Park, C. B.; Lee, S. H.; Subramanian, E.; Kale, B. B.; Lee, S. M.; Baeg, J. O. *Chem. Commun.* **2008**, 5423−5425.

(6) Diwald, O.; Tompson, T. L.; Zubkov, T.; Goralski, E. G.; Walck, S. D.; Yates, J. T. *J. Phys. Chem. B* **2004**, *108*, 6004−6008.

(7) Li, D.; Kaner, R. B. *Science* **2008**, *320*, 1170−1171.

(8) Dikin, D. A.; Stankovich, S.; Zimney, E. J.; Piner, R. D.; Dommett, G. H. G.; Evmenenko, G.; Nguyen, S. T.; Ruoff, R. S. *Nature* **2007**, *448*, 457−460.

(9) Chen, H.; Muller, M. B.; Gilmore, K. J.; Wallace, G. G.; Li, D. *Adv. Mater.* **2008**, *20*, 3557−3561.

(10) Geim, A. K.; Novoselov, K. S. *Nat. Mater.* **2007**, *6*, 183−191.

(11) Zhang, H.; Lv, X.; Li, Y.; Wang, Y.; Li, J. *ACS Nano* **2010**, *4*, 380−386.

(12) (a) Williams, G.; Seger, B.; Kamat, P. V. *ACS Nano* **2008**, *2*, 1487−1491. (b) Xiang, Q.; Yu, J.; Jaroniec, M. *Chem. Soc. Rev.* **2012**, *41*, 782−796.

(13) Lee, C.; Wei, X.; Kysar, J. W.; Hone, J. *Science* **2008**, *321*, 385.

(14) Ruppert, R.; Herrmann, S.; Steckhan, E. J. *Chem. Soc., Chem. Commun.* **1988**, 1150−1151.

(15) Gao, W.; Alemany, L. B.; Ci, L.; Ajayan, P. M. *Nat. Chem.* **2009**, *1*, 403−408.

(16) Ang, P. K.; Wang, S.; Bao, Q.; Thong, J. T. L.; Loh, K. P. *ACS Nano* **2009**, *3*, 3587−3594.

(17) Niyogi, S.; Bekyarova, E.; Itkis, M. E.; McWilliams, J. L.; Hamon, M. A.; Haddon, R. C. *J. Am. Chem. Soc.* **2006**, *128*, 7720−7721.

(18) Kaniyoor, A.; Baby, T. T.; Ramaprabhu, S. *J. Mater. Chem.* **2010**, *20*, 8467−8469.
(19) Ferrari, A. C.; Meyer, J. C.; Scardaci, V.; Casiraghi, C.; Lazzeri, M.; Mauri, F.; Piscanec, S.; Jiang, D.; Novoselov, K. S.; Roth, S.; Geim, A. K. *Phys. Rev. Lett.* **2006**, *97*, 187401.
(20) Watcharotone, S.; Dikin, D. A.; Stankovich, S.; Piner, R.; Jung, I.; Dommett, G. H. B.; Evmenenko, G.; Wu, S-E; Chen, S-F; Liu, C-P; Nguyen, S. T.; Ruoff, R. S. *Nano Lett.* **2007**, *7*, 1888−1892.
(21) Rao, C. N. R.; Sood, A. K.; Subrahmanyam, K. S.; Govindaraj, A. *Angew. Chem., Int. Ed.* **2009**, *48*, 7752−7777.
(22) Zhang, X.; Feng, Y.; Tang, S.; Feng, W. *Carbon* **2010**, 211−216.
(23) Lin, Y.; Zhang, K.; Chen, W.; Liu, Y.; Geng, Z.; Zeng, J.; Pan, N.; Yan, L.; Wang, X.; Hou, J. G. *ACS Nano* **2010**, *4*, 3033−3038.
(24) Mou, Z.; Dong, Y.; Li, S.; Du, Y.; Wang, X.; Yang, P.; Wang, S. *Int. J. Hydrogen Energy* **2011**, *36*, 8885−8893.
(25) Kresse, G.; Hafnere, J. *J. Phys. Rev. B* **1993**, *47*, 558.
(26) Zhang, Y.; Tan, Y.-W.; Stormer, H. L.; Kim, P. *Nature* **2005**, *438*, 201−204.
(27) Palummo, M.; Hogan, C.; Sottile, F.; Bagala, P.; Rubio, A. *J. Chem. Phys.* **2009**, *131*, 084102−1-084102−7.
(28) Hummers, W. S., Jr.; Offman, R. E. *J. Am. Chem. Soc.* **1958**, *80* (6), 1339.
(29) Tao, M.; Liu, L.; Liu, D.; Zhou, X. *Dyes Pigm.* **2010**, *85*, 21−26.
(30) Fungo, F.; Otero, L. A.; Sereno, L.; Silber, J. J.; Durantini, E. N. *Dyes Pigm.* **2001**, *50*, 163−170.